SMALL-CRACK GROWTH BEHAVIOR IN HIGH-STRENGTH ALUMINUM ALLOYS
-A NASA/CAE COOPERATIVE PROGRAM

J. C. Newman, Jr.[1], X. R. Wu[2], M. H. Swain[3],
W. Zhao[2], E. P. Phillips[1] and C. F. Ding[2]

Abstract

The National Aeronautics and Space Administration (NASA) and the Chinese Aeronautics and Astronautics Establishment (CAE) participated in a Fatigue and Fracture Mechanics Cooperative Program to study the "small-crack" effect in high strength aluminum alloys. Both experimental and analytical investigations were conducted to study crack initiation and growth of small cracks in bare 7075-T6 and clad LC9cs aluminum alloys, to improve fracture mechanics analyses of surface- and corner-crack configurations, and to develop improved life-prediction methods to correlate and predict small- and large-crack growth under various load histories.

Fatigue tests on single-edge-notch-tension (SENT) specimens, small-crack tests on SENT specimens, and large-crack tests on center-crack tension specimens were conducted under constant-amplitude (stress ratios of -1, 0 and 0.5) and Mini-TWIST spectrum loading. The initiation and growth of small fatigue cracks at a semi-circular notch were monitored using the plastic-replica method. Large crack-growth rate data for cracks greater than 2 mm in length were obtained over a wide range in rates for all constant-amplitude loading conditions. Crack-growth results from both laboratories agreed well. A pronounced small-crack effect was observed in both materials, especially for the negative stress ratio tests. For all loading conditions, most of the fatigue life of the SENT specimens was shown to be crack propagation from a material defect (inclusion particles or voids) or from the cladding layer.

In the analytical program, three-dimensional finite-element and weight-function methods were used to determine stress-intensity factors for surface and corner cracks at the notch in the SENT specimen. Results from the two analysis methods generally agreed within ± 3 %. Stress-intensity factor equations were developed and used in a crack-growth and crack-closure model to correlate small- and large-crack data and to make fatigue-life predictions. Predicted crack-growth rates and fatigue lives agreed well with experiments.

I. Introduction

Fatigue failure in metallic materials has, historically, been divided into three phases: crack initiation, crack growth and fracture. The use of fracture-mechanics concepts to characterize the growth of large cracks and fracture is well established in the design of aerospace structures. During the past decade, attention has been focused on extending these concepts to much smaller crack sizes. However, experimental data and analyses[1-16] have shown that linear-elastic fracture mechanics concepts break down for small cracks (less than 1 mm in length) and that the data will exhibit a small-crack effect, as shown in Figure 1. When small-crack growth rates, da/dN, are plotted against ΔK, they show that small cracks grow faster than large cracks at the same ΔK level
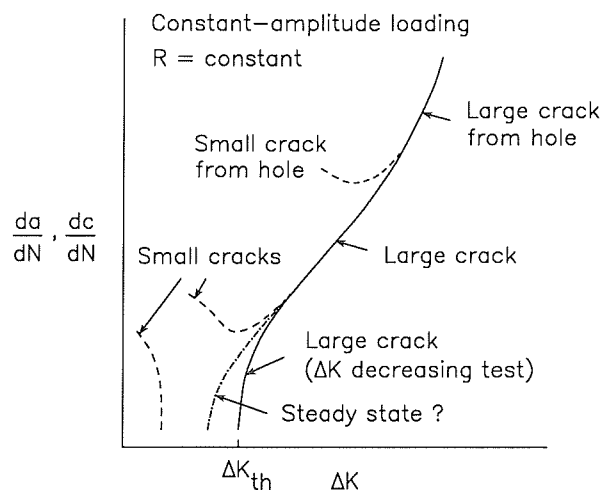

Figure 1. Typical fatigue-crack growth rate data for small and large cracks.

---

1 NASA Langley Research Center, Hampton, Virginia, USA.
2 CAE, Beijing Institute of Aeronautical Materials, Beijing, P. R. China.
3 Lockheed Engineering and Sciences Co., Hampton, Virginia, USA.

and that they also grow at ΔK levels below the large-crack threshold, ΔK_{th}. Small cracks may exhibit a variety of behaviors depending upon material and applied stress levels as indicated in Figure 1. Explanations for the small-crack effect are usually based on the argument that ΔK is not an appropriate parameter to characterize the crack-driving force for small cracks because either: (1) the basic assumptions of the ΔK concept regarding plasticity[3,4] or continuum mechanics[7,10,11] are violated at small-crack sizes or (2) the magnitude of crack-tip shielding (or closure) is very different for small and large cracks.[5,9,12] Because large-crack thresholds may also be affected by a rise in closure behavior, the steady-state crack-growth rate behavior (dash-dot curve) may lie between small- and large-crack data.

A crack size must exist below which the assumptions of continuum mechanics and the ΔK-concept are violated. However, the transition from valid to invalid conditions does not occur abruptly. A ΔK-based analysis that extends into the "gray area" of validity may still prove to be very useful. From a designer's viewpoint, a single analysis method that is applicable to all crack sizes is very desirable, as demonstrated in a total-life analysis in Reference 13. If for no other reason than that ΔK analyses are already being used for large-crack problems, the application of a ΔK analysis to small-crack problems should be thoroughly explored. The approach in this report is to apply continuum mechanics concepts, ΔK analyses, and the crack-closure concept to small- and large-crack growth.

II. Cooperative Program Overview

In May of 1985, the National Aeronautics and Space Administration (NASA) and the Chinese Aeronautics and Astronautics Establishment (CAE) held a Symposium on Structural Analysis Methods in Beijing, China. During technical discussions, several research areas of mutual interest were identified for technical cooperation. The subjects of "small-crack" growth and the break down of linear-elastic fracture mechanic concepts were identified as important problems to the aerospace industry. The CAE had recently developed some simple weight-function methods for analyzing cracks in two-dimensional cracked bodies. At that time, some newly emerging three-dimensional weight-function methods for conducting stress analyses of surface and corner cracks at stress concentrations offered an excellent opportunity to compare these analyses with some existing methods and solutions developed by NASA using finite-element methods. In addition, the development by NASA of an improved life-prediction method based on the crack-closure

concept offered an opportunity to develop a research plan between the two organizations. A joint technology plan on fatigue and fracture mechanics was established during late 1986 and early 1987. The objectives of this plan were to study the regime of small-crack growth, to develop a link between classical S-N fatigue behavior and modern damage-tolerance methodologies, to bridge "durability" and "damage-tolerance" analyses, to improve life-prediction capabilities by developing more accurate stress-intensity factor solutions for small cracks, and to evaluate an existing analytical model to predict the growth of such cracks. The complete details of the cooperative program are being published in Reference 17 and a condensed version of the program results is presented herein.

Two high-strength aluminum alloys, 7075-T6 bare and LC9cs clad sheet, were selected for the study. Three types of tests were conducted: fatigue tests on single-edge-notch-tension (SENT) specimens, small-crack tests on the SENT specimen, and large-crack tests on center-crack tension (CCT) specimens. The initiation and growth of small fatigue cracks (10 μm to 2 mm) from the edge of a notch were monitored under various load histories using the plastic-replica method. Tests were conducted under several constant-amplitude and spectrum loading conditions. Large crack-growth rate data for cracks greater than 2 mm in length were obtained for all loading conditions.

Three-dimensional (3D) finite-element and weight-function methods were used to determine stress-intensity factors for surface and corner cracks at the notch in the SENT specimen, as shown in Figures 2. Comparisons were made between the results from these two methods over a wide range in crack-configuration parameters. A description of

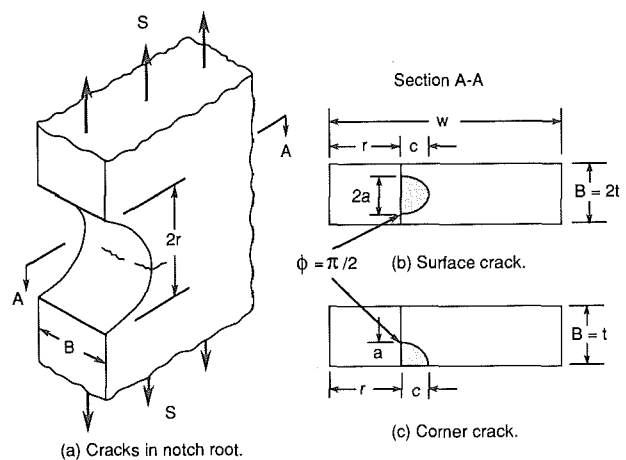(a) Cracks in notch root.

(b) Surface crack.

(c) Corner crack.

Figure 2. Single-edge-notch-tension (SENT) fatigue specimen with surface and corner crack.

the 3D finite-element methods and the 2D and 3D weight-function methods are given in Reference 17. An indirect boundary-element method, the Boundary-Force Method (BFM), was also used to obtain stress-intensity factors for through cracks in the SENT specimen.[18] Results from the BFM were compared with experimental stress-intensity factors to determine remote boundary conditions on the SENT specimen. Stress-intensity factor equations for surface, corner and through cracks at the notch were developed for a wide range in crack-configuration parameters.[17] These equations were used in the small-crack data correlations and in fatigue-life predictions.

A crack-growth model, incorporating crack-closure effects, was used to analyze the growth of small cracks along the bore of the notch and of large cracks away from the notch.[19,20] Small cracks were assumed to initiate from inclusion-particle clusters (surface cracks) or from the cladding layer (corner cracks) in these materials. Comparisons were made between experimental and predicted surface- and corner-crack shape changes, small-crack growth rates, large-crack growth and total fatigue life under constant-amplitude and spectrum loading.

III. Experimental Program

Three types of fatigue tests were conducted under constant-amplitude and spectrum loading. Standard fatigue tests on the SENT specimens were conducted to determine the S-N (stress-cycles) curves for the two materials (7075-T6 bare and LC9cs clad), especially near the endurance limit. Small-crack tests were conducted on the SENT specimens using stress levels that were selected from the fatigue test results. Large-crack tests on center-crack tension specimens were also conducted to determine fatigue crack-growth rate data over a wide range in rates. These tests were conducted under the same loading histories as the small-crack tests. All tests were conducted at room temperature and under laboratory air conditions.

Materials

Two high-strength aluminum alloy sheet materials commonly used for aircraft structures were selected for the test program. One material was 7075-T6 aluminum alloy sheet (2.3 mm thick) and the other was LC9cs clad aluminum alloy sheet (2 mm thick). The 7075-T6 material was selected because the growth of small cracks was expected to be impeded by grain boundaries [7,11] and would severely test continuum mechanics concepts. The LC9cs clad sheet material, similar in chemical composition and tensile properties to 7075-T6, was

selected because clad material is used extensively in the aircraft industry. The LC9cs sheet has a cladding layer 80 to 100 μm thick on each surface of the sheet. The cladding layer thickness was reduced to about 50 to 70 μm after chemical polishing of the SENT specimens. The thin cladding layer, composed mainly of Al-Zn, is used to enhance corrosion resistance. The tensile strength of the cladding material is only about 10 percent of the bare material. Yield stress and ultimate tensile strength of the bare LC9 material were 514 and 575 MPa, respectively, for the 7075-T6 material they were 520 and 575 MPa, respectively.

Microstructures typical of each material showed similar clusters of inclusion particles in both the 7075-T6 and bare LC9 materials. The cladding layer was cleaner than the bare material but still contained many small inclusion particles. Both bare materials had a similar pancake grain structure with the smallest dimension (about 7 μm) in the sheet thickness direction.

Specimen Configurations

The "small-crack" specimen was selected to produce naturally-occurring cracks at material defects or discontinuities and to propagate cracks through a stress field similar to that encountered in aircraft structures. A single-edge-notch-tensile specimen, as shown in Figure 2, was used. The notch was semi-circular with a radius (r) of 3.2 mm, the specimen width (w) was 50 mm and the distance between grip lines was 150 mm. The stress-concentration factor was 3.15 based on gross-section stress. The normal stress distribution near the notch root of the SENT specimen is similar to that for an open hole in a large plate. However, the edge notch permitted easy assess to the notch surface, thus making crack monitoring by the plastic-replica method convenient.

Chemical polishing of the SENT specimens was performed to debur the edge of the notch, to remove machining marks from the notch surface, and to remove a thin layer of material that might still contain residual stresses. The polishing process removed about 20 μm of material from all surfaces. In a few specimens, the notch root residual stresses were measured by X-ray diffraction. These measurements indicated that the residual stress was negligibly small (only 1 to 2 MPa).

All large-crack tests were conducted on 150-mm wide center-crack tension specimens made of the two materials in the as-received condition. The LC9cs specimens had cladding about 90 μm thick on each surface of the specimen.

Loading Conditions

A wide range in loading conditions were applied in the test program. Fatigue, small-crack and large-crack tests were conducted under three constant-amplitude loading conditions (stress ratio $R = S_{min}/S_{max} = -1$, 0 and 0.5) and under a standardized aircraft wing spectrum, Mini-TWIST. Each laboratory was required to align their test machines and gripping fixtures to produce a nearly uniform tensile stress field on an un-notched sheet specimen instrumented with strain gauges. Anti-buckling guides lined with teflon sheets were used on all tests where compressive loads were applied. The cyclic frequencies ranged from 5 to 20 Hz for the fatigue and small-crack tests. Test frequencies for the large-crack tests ranged from 5 to 30 Hz for constant-load tests and 30 to 50 Hz for the threshold (load-shedding) tests.

Mini-TWIST is a European standard gust load sequence for flight simulation tests on transport aircraft wing structures. The standardized flight load sequence represents 4000 flights. Stress levels in each flight have been normalized by the one-g stress level S_{mf} (mean stress in flight) under cruise conditions. The severest flight has one occurrence at the highest peak level ($S_{max} = 2.6 \ S_{mf}$). The lowest trough (or minimum stress) in the total sequence is $S_{min} = -0.6 \ S_{mf}$. The cumulative number of load cycles per block of 4000 flights and landings for Mini-TWIST is 62,442 cycles. Reference 21 gives a complete Mini-TWIST sequence in flight types and gives a FORTRAN listing of a program to generate the sequence. To ensure that the Mini-TWIST load sequences and magnitudes were identical for both laboratories, the same load-generator code was used at NASA and the CAE.

Fatigue (S-N) Tests

Standard fatigue (S-N) tests were conducted on the SENT specimens at various maximum stress levels (S_{max}) under both constant-amplitude and spectrum loading. These tests were used to aid in the selection of the applied stress levels and plastic-replica intervals to be used in the small-crack growth rate tests. The fatigue life data were also used to assess a total-fatigue-life prediction method based solely on crack propagation from material microstructural defects or from the cladding layer.

Small-Crack Tests

There were two objectives for the small-crack tests: (1) obtain surface-crack-length- or corner-crack-length-against-cycles data, and (2) obtain surface-crack or corner-crack shape information. To achieve these objectives, two types of tests

were required. Some specimens were tested to obtain crack-length-against-cycles data until one continuous crack extended across the notch root and the specimen was then pulled to failure. Other specimens were tested until the total crack length along the bore of the notch was much less than the sheet thickness and the specimen was then pulled to failure. The fracture surfaces were examined to reveal the surface- or corner-crack (or cracks) shapes.

The plastic-replica method was used to monitor the growth and location of single and multiple cracks along the bore of a notch.[22] This method has been found to be accurate down to the small crack lengths required in the program. The method is very simple to apply, but is very labor intensive because many replicas have to be taken to adequately describe crack length against cycles behavior. Replicas were taken at a cyclic interval chosen so that at least 25 to 30 replicas were taken during each test. Replicas were taken while the specimen was under tensile load (0.6 to 0.8 S_{max}). Figure 3 shows examples of scanning-electron-microscope (SEM) photographs of replicas of the notch surface for the two materials. Crack length measurements L were the horizontal projections. For surface cracks, the measured length L is equal to 2a and for corner cracks, L is equal to a. The test was terminated when the crack had grown across the total specimen thickness, B. During many tests, multiple cracks initiated along the notch root. Because multiple-crack interaction is beyond the scope of this report, a crack non-interaction criteria[17] was developed and used to exclude data from interacting cracks.

Large-Crack Tests

Fatigue-crack-growth-rate tests were conducted for large cracks (lengths greater than 2 mm) at the three constant-amplitude stress ratios and under the Mini-TWIST load sequence. Fatigue-crack-growth-rate data was generated for the two materials over a wide range in rate, especially in the near-threshold crack growth regime. Tests were conducted on 150 mm-wide center-crack tension specimens made of the two materials. These data were used to define the regime where small-crack data from the SENT specimen correlated with large-crack data.

Constant-amplitude tests were conducted at stress ratios (R) of -1, 0 and 0.5. At each stress ratio, two types of tests were conducted: constant amplitude and threshold. In the threshold tests, crack-growth rate data was obtained using a load-shedding (decreasing ΔK) procedure. The load-shedding procedure used by NASA (6 percent load
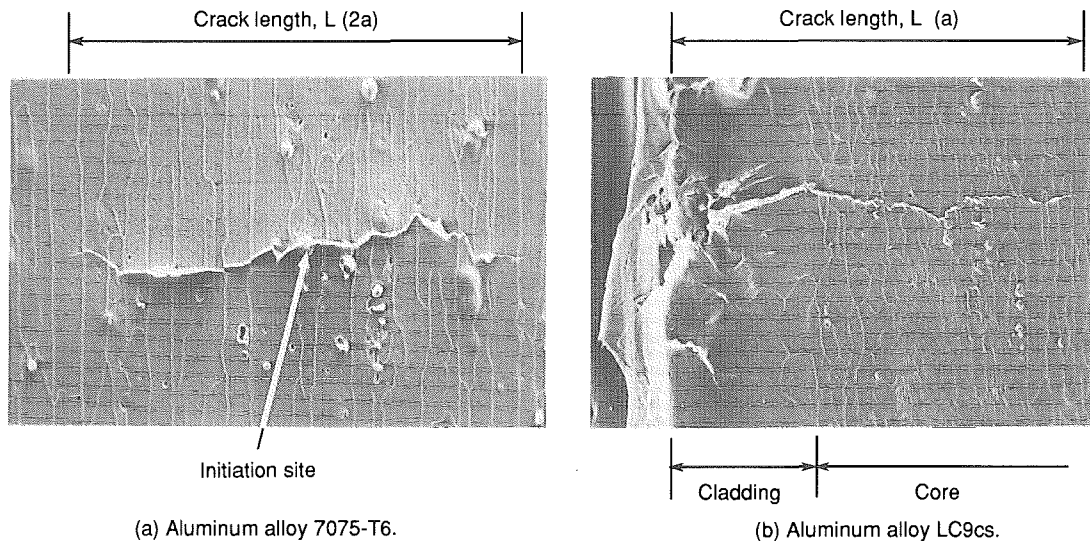
Figure 3. Scanning-electron-microscope photographs of replicas showing surface- and corner-crack-length measurements in notch root.

reduction every 1 mm of crack growth) was consistent with the guidelines of the ASTM Standard Test for Measurement of Fatigue Crack Growth Rates (E647-87). The load-shedding procedure used by the CAE was similar (load was decreased by 10 percent every 1 mm of crack growth for rates greater than 2E-06 mm/cycle and 6 percent for rates lower than 2E-06 mm/cycle). After reaching threshold conditions, some specimens were then tested under load-increasing conditions to obtain more crack-growth rate data.

Spectrum tests under Mini-TWIST loading were controlled by a computer. Computer programs were written which allowed the mean flight stress to be changed at any stage during the test, to stop the test at zero load or to stop the test at the required stress level to take replicas on the SENT specimens. This program allowed load-decreasing or load-increasing tests to be conducted without interrupting the flight-history sequence by gradually changing the mean flight stress (S_{mf}).

IV. Analytical Program

To develop an understanding of small-crack growth and to improve life-prediction methods, stress-intensity factor solutions are needed for small surface and corner cracks in plates or at stress concentrations. Although many methods have been used to analyze three-dimensional crack configurations, the majority of solutions have been obtained using finite-element methods, in conjunction with various techniques to calculate stress-intensity factors, see for example References 23-29. For the SENT specimen, the only stress-intensity factor solution available for a surface crack at a notch was based on an engineering estimate.[30] The accuracy of this solution was unknown. Stress-intensity factor solutions were not available for corner cracks at a notch. A joint effort was undertaken in the analysis program to develop stress-intensity factor solutions for surface and corner cracks at the notch root of the SENT specimen. Two radically different analysis methods, finite elements and weight functions, were used.

Three-dimensional (3D) finite-element methods (FEM) and a 3D weight-function method (WFM) were used to analyze the crack configurations shown in Figure 2. The surface crack was located at the center of the semi-circular notch, Figure 2(b), and the corner crack was located at the edge of the notch, Figure 2(c). Herein, crack depth, a, is measured in the thickness (t) direction and crack length, c, is measured in the width (w) direction. Analyses of off-center surface cracks or multiple interacting cracks were not considered. Two-dimensional (2D) weight-function analyses were also used to help develop the stress-intensity factor equations used in the 3D WFM. A two-dimensional Boundary-Force Method (BFM) was used to obtain the stress distribution in an uncracked SENT specimen. This stress distribution was used in both the 2D and 3D WFM. The BFM was also used to obtain stress-intensity factors for a through crack in the SENT specimen.

Stress-intensity factor equations, fit to the calculated stress-intensity factors, were developed for a wide range in crack-configuration parameters. A clad correction for corner cracks in the LC9cs clad material was also developed.

Finite-Element Analyses

Two finite-element programs and three methods to calculate stress-intensity factors were used to determine stress-intensity factors for surface and corner cracks emanating from a semi-circular notch. The finite-element program and method (singularity element and nodal-force method) developed by Raju and Newman[23,24] were used for semi-circular and low aspect ratio (low a/c) cracks. For large aspect ratio (a/c = 2) cracks, the finite-element program (non-singular elements) developed by Shivakumar and Newman[29] and the equivalent-domain integral (EDI) method[26] were used. The virtual-crack-closure technique[27] was also used to verify stress-intensity factors for some particular cases.

The ratio of crack depth to crack length (a/c) ranged from 0.4 to 2 and the ratio of crack depth to plate thickness (a/t) ranged from 0.2 to 0.8. The hole-radius-to-plate-thickness (r/t) ratio was 3 for surface cracks and 1.5 for corner cracks. These are the nominal r/t values used in the test program for the SENT specimens made of the two materials. The FEM analyses were conducted on a super-computer using about 15,000 degrees-of-freedom (DOF). Some typical FEM stress-intensity factor solutions will be presented but all of the results are given in Reference 17.

Weight-Function Analyses

The 3D weight-function method (WFM), developed by Zhao, Wu and Yan in References 31 and 32, was based on the slice-synthesis procedure[33,34] and the expressions for two-dimensional (2D) weight functions.[35-37] A review of two- and three-dimensional weight-function methods and solutions is given by Wu and Carlsson in Reference 38. The 3D WFM has previously been applied to embedded elliptical cracks, semi-elliptical surface cracks, and quarter-elliptical corner cracks, in finite thickness plates subjected to Mode I loading. Results from the WFM agreed well with other accepted solutions for these crack configurations (see Refs. 31, 32 and 35 to 41).

Herein, the method was applied to surface and corner cracks at the semi-circular notch in the SENT specimen. The 3D WFM formulated here, however, assumed that the normal stress distribution around the notch root was uniform through the thickness. This assumption was justified for the SENT specimen configurations used in the current study because through-the-thickness variations in normal stress are small.[42] The 3D WFM can determine stress-intensity factors at any location along a crack periphery for the crack configurations shown in Figure 2. The ratio of crack depth to crack length (a/c) ranged from 0.2 to 2 and the ratio of crack depth to plate thickness (a/t) ranged from 0.05 to 0.5. The hole-radius-to-plate-thickness (r/t) ratio was 2.78 and 3.2 for surface cracks and 1.39 and 1.6 for corner cracks. These are the specific r/t values used in the test program for the two materials. Whereas the FEM analyses were conducted on a mainframe computer, the WFM analyses were performed on a personal computer. Again, some typical WFM stress-intensity factor solutions will be presented but all results are given in Reference 17.

Boundary-Force Method

The BFM was developed for conducting two-dimensional stress analyses of complex configurations, with and without a crack, subjected to internal loadings and to traction or displacement boundary conditions.[18] The BFM was based on the elasticity solution for concentrated forces and moment in an infinite plate with a crack.[43] The BFM was used to analyze the uncracked SENT specimen to obtain the stress-concentration factor and the normal-stress distribution along the net section. In addition, the BFM was used to analyze a through crack emanating from the notch in the SENT specimen subjected to either remote uniform stress or to remote uniform displacement.

Stress-Intensity Factor Equations

The FEM and WFM stress-intensity factor solutions for surface and corner cracks at a notch and the BFM solutions for a through crack at a notch were used to develop approximate equations. The stress-intensity factors for a semi-elliptical surface crack located at the center of a semi-circular edge notch and a quarter-elliptical corner crack located at the edge of the notch subjected to remote uniform stress or uniform displacement were expressed as

$$K = S \sqrt{\pi a/Q} \; F_{jn}(\frac{a}{c}, \frac{a}{t}, \frac{c}{r}, \frac{c}{w}, \frac{r}{t}, \frac{r}{w}, \varphi) \qquad (1)$$

where Q is the shape factor and F_{jn} (j = s or c) is the boundary-correction factor. F_{sn} is the boundary-correction factor for the surface crack; and F_{cn} is the correction factor for a corner crack. Equation (1) applies over a wide range in crack-configuration parameters (a/c, a/t) but is restricted to the SENT specimen with r/w = 1/16 and 1 < r/t < 3.5. This particular r/w value is for the SENT configurations used in the test program. Note that here t is defined as one-half of the full sheet thickness for surface cracks, and t is full sheet thickness for corner cracks. The equations for Q and F_{jn} are given in Reference 17.

Comparison of Methods and Equations

Some typical comparisons among the stress-intensity boundary-correction factors from the FEM, WFM and equations are shown in Figures 4 and 5 for a surface crack and corner crack at a notch, respectively. The boundary-correction factor is plotted against the parametric angle, φ. The surface crack results (Fig. 4) are for $a/c = 1$ and $r/t = 3$. The WFM results (solid symbols) are the average of results obtained for the two values of r/t (2.78 and 3.2) used in the test program. Open symbols show the FEM results and the equations are shown by the curves for various a/t ratios. The equations are within ± 3 % of the WFM and FEM results, except where the crack intersects the notch boundary ($\varphi = 90$ deg.). The drop-off in stress-intensity factor at the free surface was neglected in developing the equations and in the analyses of surface- and corner-crack growth.
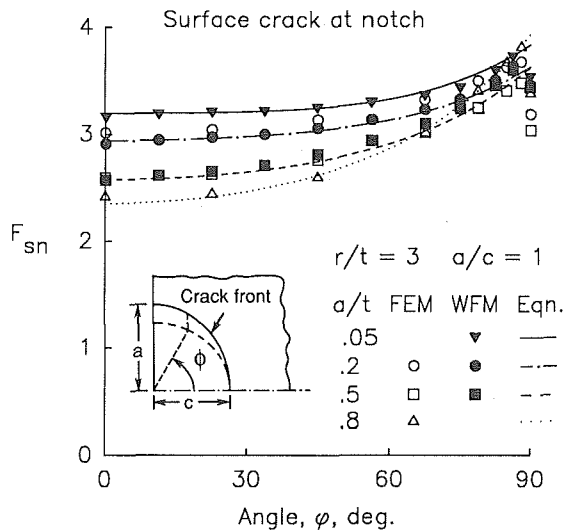
The stress-intensity boundary-correction factors from the FEM, WFM and equations for a corner crack at the notch root in the SENT specimen are shown in Figure 5. This figure shows results for $a/c = 1$ and $r/t = 1.5$ Again, the WFM results (solid symbols) are the average of results obtained for the two values of r/t (1.39 and 1.6). Open symbols show the FEM results for $r/t = 1.5$ and the corner-crack equations are shown by the curves. The WFM results are generally within ± 3 % of the FEM results. The equation is about 2 to 5 % lower than the WFM for a shallow ($a/t = 0.05$) crack. Some larger differences (about 10 %) were observed between the WFM and FEM results for shallow cracks with $a/c = 2$ and for deep cracks with $a/c = 0.4$, as described in Reference 17. In general, however, the agreement between the WFM and FEM was very good (within ± 3 %) for the wide range in crack configurations considered in the program.

The stress-intensity factor for a through crack emanating from the semi-circular notch subjected to remote uniform stress or uniform displacement is expressed as

$$K = S \sqrt{\pi c} \; F_{tn}(\tfrac{c}{w}, \; \tfrac{c}{r}, \; \tfrac{r}{w}) \qquad (2)$$

where F_{tn} is the boundary-correction factor for a SENT specimen with $r/w = 1/16$. The equations for F_{tn} under remote uniform stress or displacement are given in Reference 17.

Figure 6 compares the stress-intensity boundary-correction factors from the BFM and from tests for through cracks at the notch in a SENT specimen with a specimen-height-to-width (h/w) ratio of 1.5. The specimen height was measured from the specimen centerline to the grip line. The BFM results for uniform stress and uniform displacement boundary conditions are shown by the two curves. These results show that the boundary-correction factor is strongly influenced by the remote boundary condition for large crack lengths. The experimental stress-intensity boundary-correction factors, determined from fatigue-crack-growth-rate tests using the James-Anderson technique (see Ref. 44), agreed well with the BFM results for remote uniform displacement boundary conditions. Thus, the equations developed from the BFM results for uniform displacement with $h/w = 1.5$ were used in the life-prediction code[45] to predict small- and large-crack growth in the SENT specimen.

Figure 4. Comparison of boundary-correction factors from finite-element and weight-function methods for surface crack at notch.
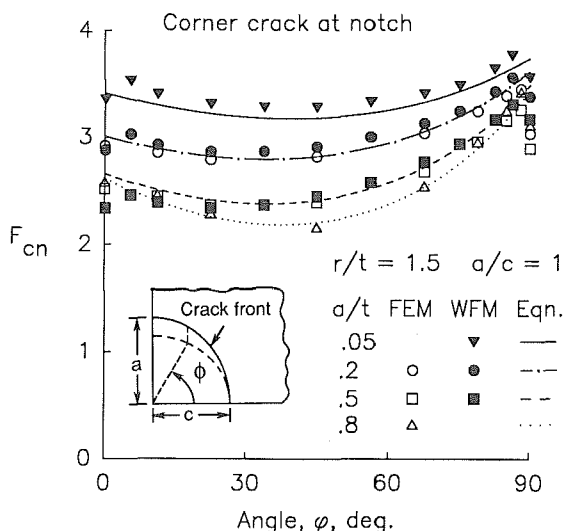

Figure 5. Comparison of boundary-correction factors from finite-element and weight-function methods for corner crack at notch.
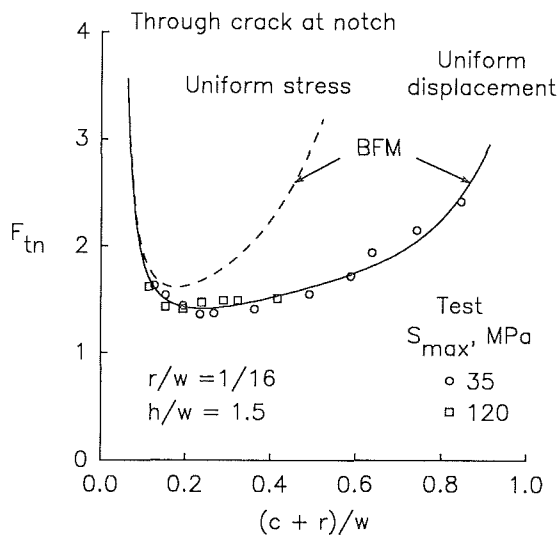
Figure 6. Comparison of boundary-correction factors from boundary-force method and tests for through crack at notch.

Effect of Cladding

In the LC9cs material, cracks initiated in the cladding layer and grew as corner cracks into the core material. To account for this behavior, the stress-intensity factor solution for corner cracks was modified to approximately model cracks in a multiple layer medium. The yield stress of the cladding was estimated to be about 50 MPa. In the SENT specimens, the cladding layer always yielded and developed multiple cracks from slip-band formation along the edges of the notch. Thus, as a first approximation, the cladding layer, with a thickness of ℓ, was assumed to carry no load. To estimate the effects of the cladding layer on stress-intensity factors, two stress-intensity factor solutions were used. One was an edge crack in a two-dimensional body with uniform stress acting only over the portion of the crack in the core material (K_{ce}) that was determined from the 2D WFM.[38] And the other was an edge crack in a homogeneous body with uniform stress acting over the entire crack (K_e).[46] A clad-correction factor was then defined as the ratio of the two solutions as

$$G_c(\ell/a) = K_{ce}/K_e \tag{3}$$

The clad-correction equation for $G_c(\ell/a)$ is given in Reference 17. If the crack depth, a, is equal to the clad thickness ($\ell/a = 1$), then $G_c = 0$. If the crack depth is large compared to clad thickness, G_c approaches unity and the cladding has no effect on stress-intensity factors. The clad-correction factor G_c was applied to all locations along the corner-crack configuration. Thus, the boundary-correction factor for the corner crack

(boundary and clad) was $F'_{cn} = F_{cn}G_c$.

V. Crack-Closure Analyses

Numerous investigators have suggested and verified that crack closure (or the lack of crack closure in the early stages of crack initiation) is a major factor in causing some of the differences between the growth of small and large cracks. Reference 47 has shown that a large part of the small-crack effect in an aluminum alloy could be explained using a crack-closure model and the assumption that cracks emanate from a "void" at inclusion particle sites. In the cooperative program, the crack-closure model[19,48] was used to calculate crack-opening stresses, to correlate large-crack growth rate data under constant-amplitude loading, to predict large-crack growth under spectrum loading, to predict small-crack growth rates, and to predict fatigue lives. In the following, some results from the model under constant-amplitude and spectrum loading will be presented.

Constant-Amplitude Loading

The crack-closure model was used to calculate crack-opening stresses under various constant-amplitude loading conditions. Some typical results that show the influence of the initial defect "void" size and stress ratio (R) on the crack-closure behavior of small fatigue cracks emanating from these voids are shown in Figure 7. Here, the calculated crack-opening stress (S'_o) normalized by the maximum applied stress is plotted as a function of crack depth, a. An initial material defect size a_i of 3 μm and c_i of 9 μm was selected for the crack-growth simulations. The defect half-height, b, was selected as 0.5 μm. The 0.5 μm value was selected so that the defect surfaces would not close even under the R = -1 compressive loading. Values of S_{max}/σ_o used in the simulations are as
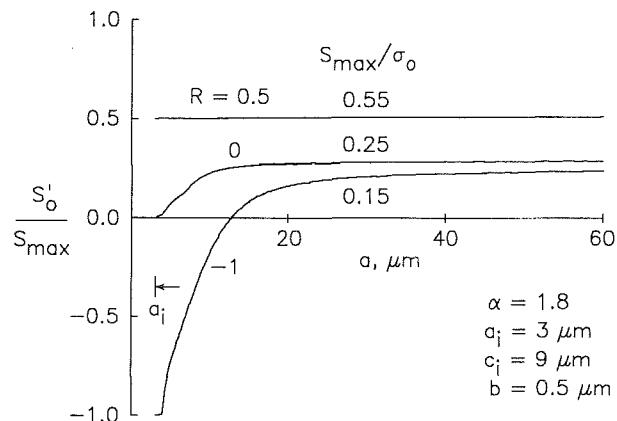

Figure 7. Calculated crack-opening stresses for constant-amplitude loadings as a function of crack length for a small crack.

indicated. The constraint factor (α) was selected to be 1.8 for this crack-growth simulation. The constraint factor accounts for the state-of-stress in the crack-front region and can vary from plane stress ($\alpha = 1$) to simulated plane-strain conditions ($\alpha = 3$), see References 19 and 47 for further details. Results from the negative stress ratio simulation (R = -1) show a significant transient in crack-closure behavior. However, at positive stress ratios, the crack-opening stresses stabilize after a very small amount of crack growth. The results at the high stress ratio (R = 0.5) show that the small-crack surfaces were always fully open. These results are important because the ΔK values under high stress-ratio conditions are the same as the ΔK_{eff} values and tests under these conditions can be used to help establish the ΔK_{eff}-rate relationship for the material of interest. The effective stress-intensity factor range[20] is defined by

$$\Delta K_{eff} = K_{max} - K'_o = \Delta K \ (1 - S'_o/S_{max})/(1 - R) \qquad (4)$$

where K'_o is the stress-intensity factor at the crack-opening stress, S'_o. Tests at the lower stress ratios can then be used to help establish the proper constraint factor to correlate the crack-growth rate data as a function of ΔK_{eff}.

Mini-TWIST Spectrum Loading

One of the most important features of the crack-closure model and life-prediction code [45] is the ability to calculate the influence of load history on crack-opening stresses. Some typical crack-opening stresses under the Mini-TWIST load sequence for a small surface crack in a 7075-T6 SENT specimen are shown in Figure 8. The same initial defect size (a_i,c_i,b) used for the constant-amplitude loading was also used here. A variable-constraint option was selected for this
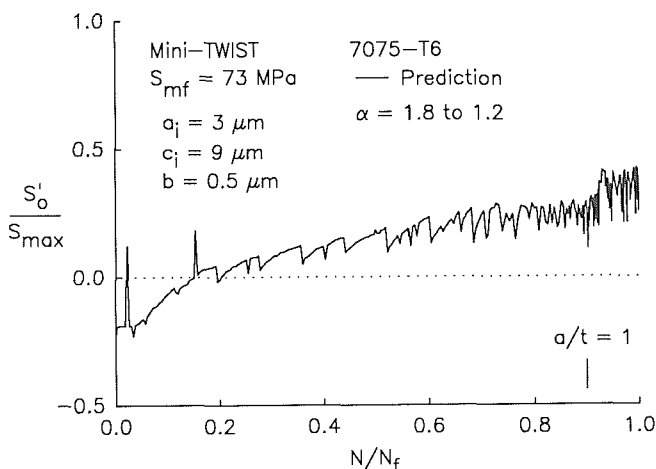

Figure 8. Calculated crack-opening stresses for a small crack under Mini-TWIST loading as a function of applied cycles.

simulation. The constraint factor (α) was 1.8 for crack-growth rates less than 7E-04 mm/cycle and 1.2 for rates greater than 7E-03 mm/cycle (variable α will be discussed later in the Large-Crack Data and Analyses section). The mean flight stress in the Mini-TWIST spectrum was selected to be 73 MPa (S_{max}= 190 MPa). The figure shows crack-opening stress (normalized by the peak stress in the spectrum) plotted against the ratio of N, applied cycles, to N_f, the predicted cycles to failure. N_f was about 800,000 cycles for this case. Only a sampling of the opening stresses calculated from the model is shown in the figure. Again, the opening stresses start near the minimum stress in the spectrum and rise as the crack grows. Crack-opening stresses tend to level off for N/N_f between 0.6 and 0.9. The rapid jump in S'_o/S_{max} at an N/N_f ratio of about 0.92 was caused by the change in constraint from 1.8 to 1.2. As indicated in the figure, the surface crack became a through crack (a/t = 1) at an N/N_f ratio of about 0.9.

Crack-Opening Stress Equations

Crack-opening stress equations for constant-amplitude loading have previously been developed to help determine the ΔK_{eff} against crack-growth rate relation for any given material, thickness and environmental condition.[48,49] These equations were developed from results from the crack-closure model and give crack-opening stress as a function of stress ratio, stress level, and the constraint factor, α. These equations will not be presented here but they were used to correlate large-crack growth rate data on the basis of the effective stress-intensity factor.

Surface- and Corner-Crack Growth

Early studies on crack growth predictions of surface and corner cracks demonstrated that their growth could not be predicted solely by stress-intensity factor ranges.[50] The stress-intensity factor range at a location where a crack front intersects a free surface was multiplied by a factor β_R to account for the crack closure differences between the interior and free-surface locations. Assuming that the conditions at the free surface were plane stress and at the interior locations were plane strain, a crack-closure factor ratio (β_R) was derived and is given by

$$\beta_R = 0.9 + 0.2 \ R^2 - 0.1 \ R^4 \qquad (5)$$

for R $\geq$ 0. For R < 0, β_R is 0.9.

VI. Large-Crack Data and Analyses

Fatigue crack growth rate tests were conducted on large cracks under three constant-amplitude stress ratios and the Mini-TWIST load sequence. The objective was to generate fatigue crack growth rate (ΔK-rate) data for the two aluminum alloy materials over a wide range in rates, especially in the near-threshold crack growth regime.

The crack-closure model was then used to correlate the large-crack constant-amplitude data on the basis of the effective stress-intensity factor range.[20] The ΔK_{eff} against crack-growth rate relation was used with the crack-closure model to predict crack-length-against-cycles for the spectrum tests. Comparisons are made between experiments and spectrum predictions. The crack-growth rate data generated on large surface and corner cracks in the SENT specimens were also used to obtain ΔK_{eff}-rate relations for cracks growing in the sheet-thickness direction. These relations will also be used later to predict small-crack growth and fatigue life under the various load histories.

Constant-Amplitude Loading

Constant-amplitude fatigue-crack growth rate tests on 7075-T6 and LC9cs aluminum alloy sheets were conducted at stress ratios (R) of -1, 0 and 0.5. At each stress ratio, two types of tests were conducted: (1) constant-amplitude loading and (2) threshold (load-shedding) tests. Crack-growth rates from large-crack tests were calculated by using the secant (point-to-point) method. The stress-intensity factor range was computed from the well-known equation for a central crack in a strip under tension.[46] The equation is

$$\Delta K = \Delta S \sqrt{\pi c \, \sec(\pi c / 2w)} \qquad (6)$$

where ΔS is the full cyclic range, c is the average of the crack length measured on the right and left sides of the specimen and w is one-half of the specimen width ($w = 75$ mm).

The large-crack ΔK-rate data for the 7075-T6 material are shown in Figure 9. For each stress ratio, the data from the two laboratories agreed well but the NASA data showed slightly higher ΔK-thresholds than the CAE data for R = 0 and -1. The data at the three stress ratios form parallel bands with the higher R-ratio showing higher rates for a given ΔK. The data at each stress ratio also showed several "knees" or transitions with distinct changes in the ΔK-rate slope. These transitions tended to occur at nearly the same crack-growth rates for all R-ratios tested. References 51 and 52 showed for 7000 series and 2024 aluminum alloys,
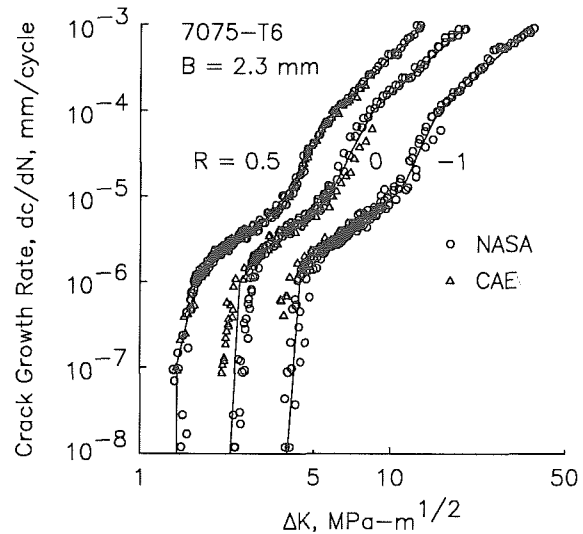

Figure 9. Crack-growth rate against ΔK for 7075-T6 alloy under constant-amplitude loading.

respectively, that these transitions correspond to loading conditions where the monotonic or cyclic plane-strain plastic-zone sizes become equal to characteristic microstructural features such as dispersoid spacings, dislocation cells, and subgrain or grain sizes. The solid lines were drawn through the data using a visual fit. These lines will be used later in comparisons made with the small-crack data.

The large-crack ΔK-rate data on the LC9cs clad material is shown in Figure 10. In calculating ΔK, the full specimen thickness was used. Again, the data from both laboratories agreed well for each R-ratio tested and the NASA data showed slightly higher ΔK-thresholds than the CAE data.
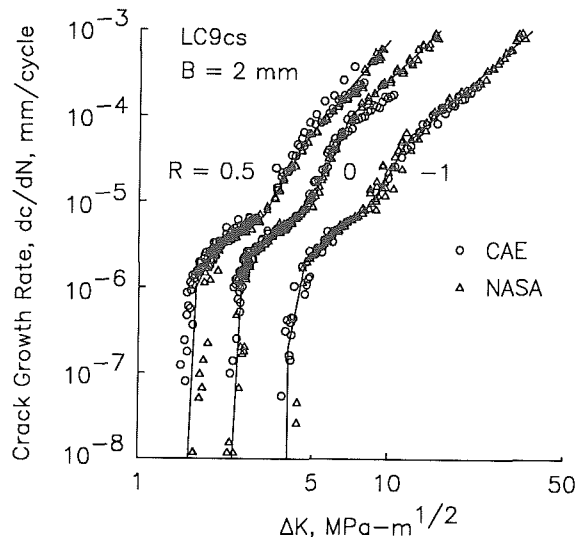

Figure 10. Crack-growth rate against ΔK for LC9cs alloy under constant-amplitude loading.

Transitions, such as those observed in the 7075-T6 data, were also observed in the clad alloy. These transitions occurred at about the same rates as those measured for the 7075 alloy. The solid lines were, again, drawn through the data using a visual fit.

The ΔK_{eff}-rate relation for 7075-T6 large-crack data (c-direction) is shown in Figure 11 for data generated at the three stress ratios. The data collapsed into a narrow band with several transitions in slope occurring at about the same rates for all stress ratios. Some differences were observed in the threshold regime. For these
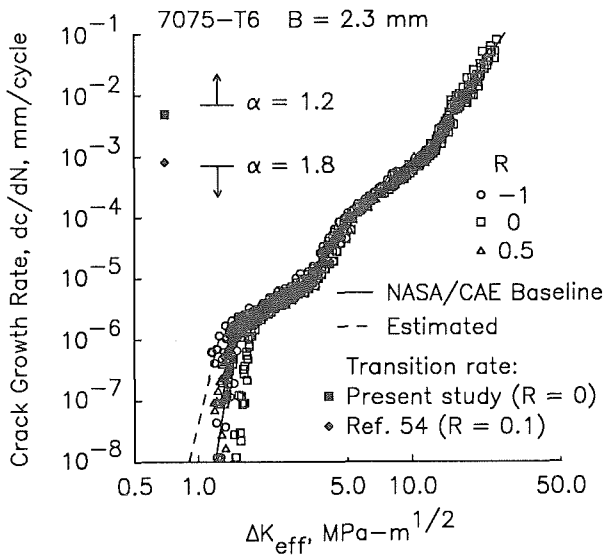
Figure 11. Effective stress-intensity factor range against growth rates for large cracks in 7075-T6 alloy for various stress ratios.

calculations, a constraint factor (α) of 1.2 was used for rates greater than 7E-03 mm/cycle (end of transition from flat-to-slant crack growth) and α equal to 1.8 (nearly equivalent to Irwin's plane-strain condition)[53] was used for rates lower than 7E-04 mm/cycle (beginning of transition from flat-to-slant crack growth). For intermediate rates, α was varied linearly with the logarithm of crack-growth rate. The solid symbols denote measured rates at the end of transition from flat-to-slant crack growth from the present study and from Vogelesang.[54] Schijve[55] has shown that the transition from flat-to-slant crack growth occurs at nearly the same crack-growth rate for a wide range in stress ratios. It has been proposed in Reference 47 that the flat-to-slant crack-growth transition region may be used to indicate a change from nearly plane-strain to plane-stress behavior and, consequently, a change in constraint. The importance of variable constraint will be shown later in crack-growth predictions made under the Mini-TWIST spectrum loading.

In the low crack-growth rate regime near and at threshold, some tests[56] and analyses[9] have indicated that the threshold develops because of a rise in the crack-opening-stress-to-maximum-stress ratio due to the load-shedding procedure. In the threshold regime then, the actual ΔK_{eff}-rate data would lie at lower values of ΔK_{eff} because the rise in crack-opening stress was not accounted for in the current analysis. Further study is needed, however, to establish the actual ΔK_{eff}-rate behavior in this regime. However, for the purpose of the current study, an estimate was made for this behavior and the relation is shown by the dashed curve. An evaluation of this estimate will be made later.

The ΔK_{eff}-rate relation for the clad alloy for growth in the c-direction is shown in Figure 12. Again, the data for the three stress ratios collapsed onto a single ΔK_{eff}-rate curve. Some differences were, again, observed in the threshold region. For these calculations, the same variable-constraint regime that was used for the 7075-T6 alloy was also used for the clad alloy. A comparison of the baseline curves for 7075-T6 and LC9cs showed that they had similar trends with the transitions in slope occurring at about the same rates. Therefore, the upper portion of the 7075-T6 data was used to extrapolate the upper portion for the clad alloy.
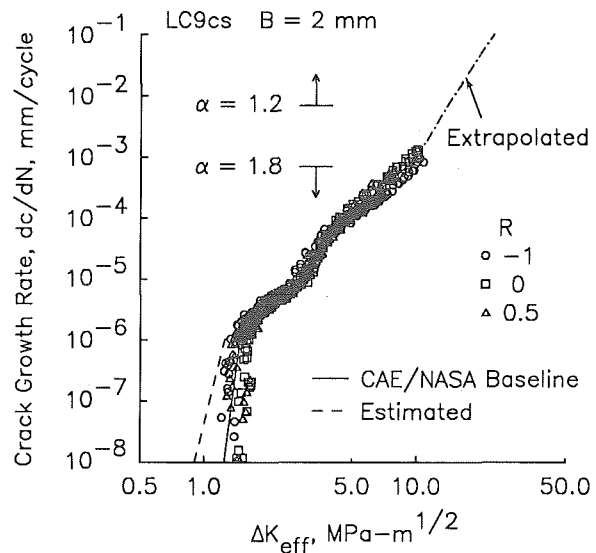

Figure 12. Effective stress-intensity factor range against growth rates for large cracks in LC9cs alloy for various stress ratios.

The surface- and corner-crack data generated on the SENT specimen under constant-amplitude loading produced crack-growth rate data in the thickness direction. Because the crack-opening stress behavior of small fatigue cracks stabilizes

after an extremely small amount of crack growth (about 40 μm for the negative stress ratio tests, see Fig. 7), these data were used to help establish crack-growth behavior in the depth (or a-direction). Using a ΔK_{eff} analysis similar to that previously discussed, baseline curves were also developed for cracks growing in the a-direction.

Multi-linear segments were used to define the baseline ΔK_{eff}-rate relations in both the a- and c-directions. A table look-up procedure was used to relate crack-growth rate to ΔK_{eff} because the baseline data can be described more accurately than with a multi-parameter equation, especially in the transitional regions. These relations were then used in the analyses to predict small- and large-crack growth rates and to predict fatigue lives under constant-amplitude and spectrum loading. The end points of these segments are listed in Tables 1 and 2.

Table 1.-Aluminum Alloy 7075-T6.

ΔK_{eff} MPa-$\sqrt{m}$	dc/dN mm/cycle	da/dN mm/cycle
0.9	1.0E-08	1.0E-08
1.25	1.0E-06	1.0E-06
3.4	1.0E-05	1.0E-05
5.2	1.0E-04	---
11.9	1.0E-03	---
14.8	---	1.0E-03
17.6	1.0E-02	---
27.5	1.0E-01	---
34.0	---	1.0E-01

Table 2.-Aluminum Alloy LC9cs.

ΔK_{eff} MPa-$\sqrt{m}$	dc/dN mm/cycle	da/dN mm/cycle
0.9	1.0E-08	1.0E-08
1.25	1.0E-06	1.0E-06
3.0	1.0E-05	1.0E-05
4.0	6.3E-05	---
10.0	1.0E-03	---
12.4	---	1.0E-03
14.8	1.0E-02	---
23.0	1.0E-01	---
28.4	---	1.0E-01

For ΔK_{eff} values below or above the extreme values listed in these tables, a power law using the first two or last two points, respectively, was used to obtain rates. The upper limit for the power-law relation is, of course, defined by fracture toughness. The fracture toughnesses were 50 MPa-$\sqrt{m}$

for both alloys. A lower limit or small-crack threshold, $(\Delta K_{eff})_{th}$, was estimated to be 0.9 MPa-$\sqrt{m}$ for both alloys on the basis of predicting the fatigue limits.

Mini-TWIST Spectrum Loading

Several tests were conducted on center-crack tension specimens to monitor large-crack growth under the Mini-TWIST load spectrum. These tests were used to evaluate the ability of the crack-closure model and life-prediction code [45] to predict large-crack growth under spectrum loading.

For the 7075-T6 alloy, five tests were conducted at three different mean-flight stress (S_{mf}) levels. These test results (symbols) are shown in Figure 13. The variable-constraint option (α varied from 1.8 at low rates to 1.2 at high rates) was used to predict spectrum crack growth. The predicted results agreed well (within ± 20 %) with all of the test results. To illustrate the importance of the variable-constraint option for spectrum crack growth in aluminum alloys, a second set of predictions (not shown) were made using a "constant" constraint factor of 1.8. The predicted results for the two lowest mean-flight stress levels were similar to those shown in Figure 13. But the predicted cycles to failure for the highest mean-flight stress level case was considerably less (about a factor of three) than the test results.
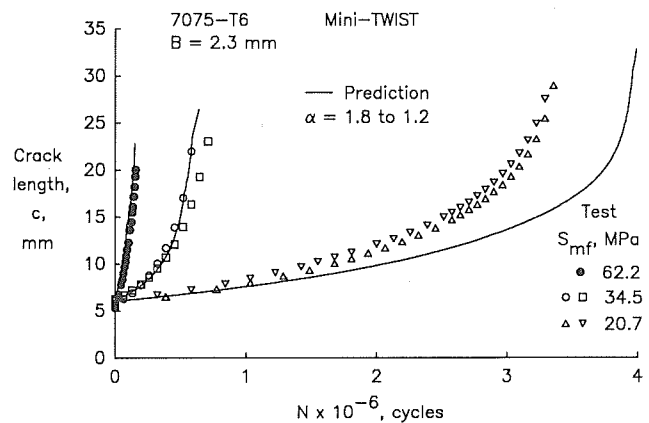

Figure 13. Comparison of experimental and predicted crack length against cycles for 7075-T6 alloy under Mini-TWIST loading.

Figure 14 shows the test results on five specimens made of the clad LC9cs alloy. Only two mean-flight stress levels were tested. The variable-constraint option was again used in making crack-length-against-cycles predictions. Because the initial crack sizes for the low mean-flight stress level tests varied, the smallest and largest initial crack sizes were used to predict upper and lower bounds. Although the shape of the crack-
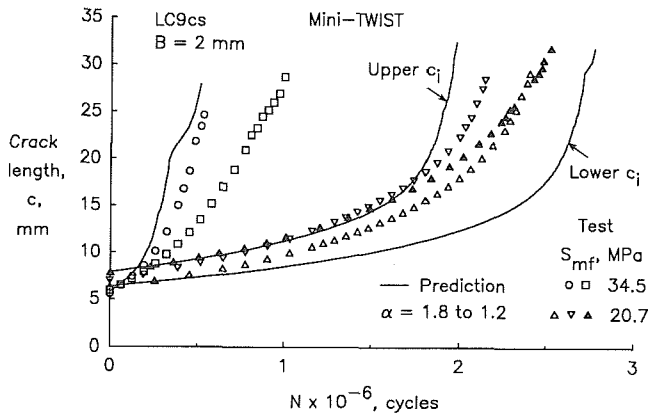
Figure 14. Comparison of experimental and predicted crack length against cycles for LC9cs alloy under Mini-TWIST loading.

length-against-cycles curves from the predictions did not match the low-stress test results near failure, the tests results generally fell between the upper and lower bounds. A large difference was observed between the two tests conducted at the 34.5 MPa mean-flight stress level. The predicted results, however, fell within a factor of two of the average of these two tests. The noticeable change in the predicted crack-length-against-cycles curve at about a 20 mm length crack was caused by one of the severe flights in the spectrum activating the low constraint value of 1.2 in the crack-closure analysis.

VII. Small-Crack Data and Analyses

In the following, test data generated on initiation sites, crack shapes, crack length against cycles, and crack-growth rates under both constant-amplitude and Mini-TWIST spectrum loading are summarized and compared with calculations or predictions made using a ΔK-based analysis and the crack-closure model.

Initiation Sites

A study of small-crack behavior must invariably consider the surface and sub-surface microstructure of the material of interest. Photographs of replicas taken at crack initiation sites along the notch-root surface are shown in Figure 3. A typical initiation site in the 7075-T6 alloy is shown in Figure 3(a). This photograph shows a surface crack initiating and growing from an inclusion cluster. Crack initiation, in general, occurred early in life at inclusion-particle clusters or voids, as observed by Bowles and Schijve.[57] In the LC9cs alloy, initiation sites were nearly always in the cladding layer as shown in Figure 3(b). Cracks also initiated early

in life and grew predominately as corner cracks. The effect of the cladding layer on fatigue behavior in aluminum alloys has been known for many years.[58] However, analysis methods have only recently been developed to analyze crack-closure behavior and crack growth for corner cracks.

The distributions of crack initiation site locations for the two alloys are compared in Figure 15. The insert in the figure shows a cross section of the notch root. The crack initiation site location, denoted as t_i, is measured from the centerline of the specimen thickness. One-half of the sheet thickness is denoted as t. The data on initiation site locations were obtained from plastic replicas taken early in life. The initiation site data from NASA and the CAE were analyzed together. The number of cracks that initiated in each of ten separate regions along the notch-root surface are plotted against t_i/t. Each region is ten percent of the specimen thickness. For 7075-T6, most of the cracks (70 %) initiated at t_i/t values less than 0.5 (middle half of specimen thickness) and tended to grow as semi-elliptical surface cracks. Crack initiation in the middle of a notch root is promoted by an elevation of stress concentration in that region.
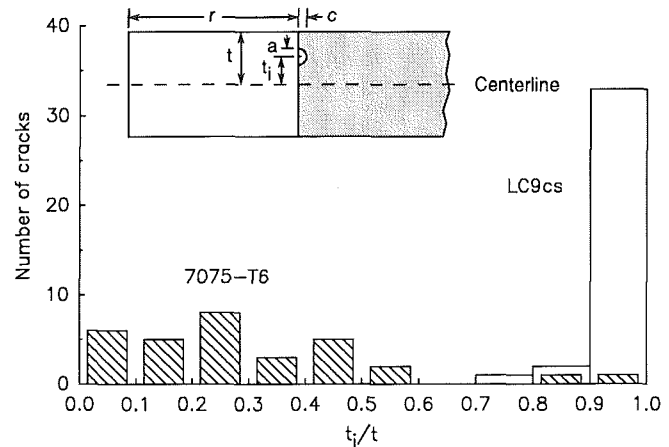

Figure 15. Distribution of crack-initiation sites along bore of notch for 7075-T6 and LC9cs alloys.

For the LC9cs alloy, more than 90 percent of the cracks initiated at the corner ($t_i/t \approx 1$) and grew as corner cracks. Thus, a corner crack was assumed in most of the analyses of small-crack growth in the clad material. In a few cases, a crack initiated as a surface crack in the LC9cs material. These few surface-crack results were very useful in assessing the influence of the cladding layer on stress-intensity factor analyses.

811

Crack Shape

The experimental and predicted crack shape changes for surface and corner cracks at the notches in 7075-T6 and LC9cs alloys are shown in Figures 16 and 17, respectively. Crack-depth-to-crack-length (a/c) ratios are plotted against the crack-depth-to-thickness (a/t) ratios. The open symbols denote test data and show some influence of stress ratio on crack shape. Results from the Mini-TWIST spectrum are also shown. The solid symbols (Fig. 16) show the size and shape of inclusion-particle clusters or voids which initiated small cracks (average size was $a_i = 3$ μm and $c_i = 12$ μm) in 7075-T6. The predicted results (curves) for all stress ratios (using the average

maximum stress level in the tests) agreed reasonably well with the test data and showed that small surface cracks tend to very rapidly approach a nearly semi-circular crack (a/c = 1). These predictions were made using the ΔK_{eff}-rate relations that differed in the a- and c-directions, as presented earlier. The sharp changes in the predicted curves were due to the sharp transitions in the ΔK_{eff}-rate curve as shown in Figure 11.

The experimental and predicted crack shape changes in the LC9cs clad alloy are shown in Figure 17. The average cladding layer thickness was about 60 μm, as indicated by the vertical line. Most cracks in the clad alloy initiated from slip-bands in the cladding layer and grew as corner cracks. For the predictions, the initial crack size was selected as 77 μm ($a_i/c_i = 1$) from experimental observations of crack sizes made early in life. Although the predicted results for the negative stress ratio agreed with the test results, those for R = 0 and 0.5 did not agree. The reason for the different trends between tests and analyses could not be determined but may be related to the approximations made in the clad correction.

Crack-Length-Against-Cycles Behavior

A plot of crack length against cycles for small cracks under constant-amplitude loading for 7075-T6 is shown in Figure 18. Negative R ratio tests were selected because small-crack effects are more pronounced under these conditions. The solid and dashed curves show test results from NASA and the CAE, respectively. The results from both laboratories agreed well. Growth of naturally-initiated cracks were detected early in life, after about 5,000 to 15,000 cycles. At these cycles, crack lengths (L) of 5 to 15 μm were measured. Although these particular tests were terminated after the crack had grown across the specimen thickness, fatigue tests to failure under these conditions would have lasted about 150,000 cycles.
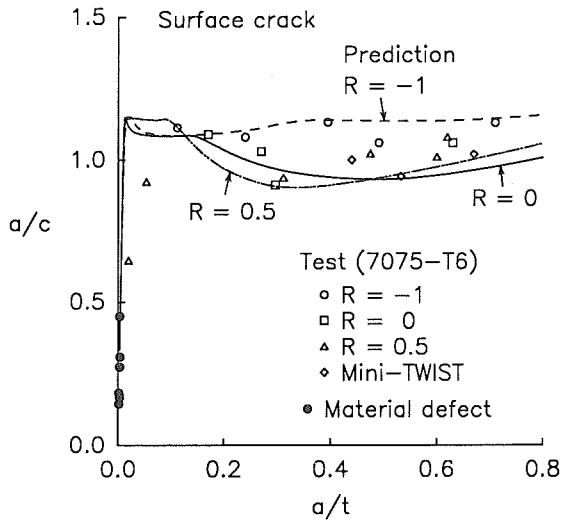
Figure 16. Comparison of experimental and predicted surface-crack shapes in 7075-T6 alloy for various stress ratios and spectrum.
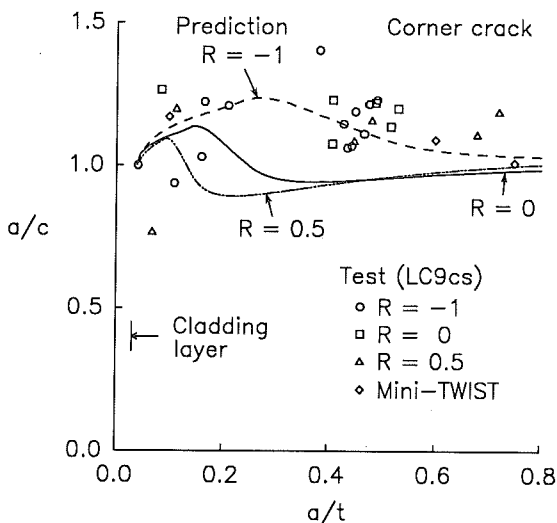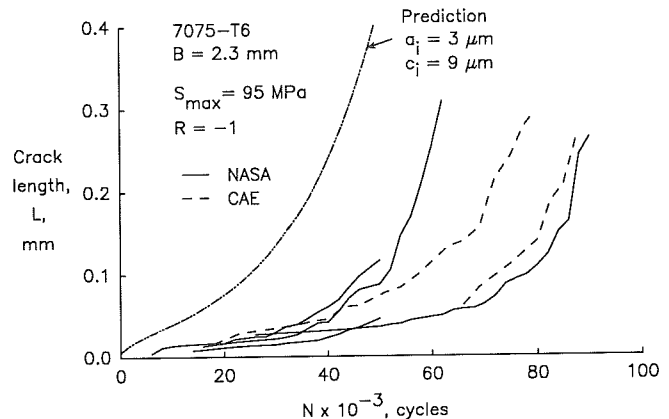
Figure 17. Comparison of experimental and predicted corner-crack shapes in LC9cs alloy for various stress ratios and spectrum.

Figure 18. Comparison of experimental and predicted small surface-crack growth in 7075-T6 alloy SENT specimens.

812

Thus, the initiation phase, cycles before a crack was detected, was only about 3 to 10 percent of the total fatigue life. In the analysis, using an initial defect size of $a_i = 3$ μm, $c_i = 9$ μm and b = 0.5 μm from typical material defect sizes, the predicted results (dashed-dot curve) fell considerably shorter than the tests. As discussed in Reference 17, the plastic-replica method had a strong influence on fatigue life (increasing life by about a factor of two at this stress level), and possibly on small-crack growth rates. It was suspected that the acetone used in the replica process reduced the moisture concentration and protected the crack-front region, resulting in longer lives. Thus, the difference shown in Figure 18 may be expected.

Crack-length-against-cycles data for small cracks in the LC9cs alloy under constant-amplitude loading conditions are shown in Figure 19. The solid and dashed curves show test results from the CAE and NASA, respectively. Again, the results from both laboratories agreed well. The clad material exhibited more scatter in fatigue life than the 7075-T6 alloy. Crack growth from naturally-initiated cracks in the cladding was also detected early in life. Crack growth was recorded as early as 1,000 cycles, but most initiated at around 4,000 cycles. At these cycles, the crack lengths (L) ranged from 60 to 100 μm. Fatigue tests under these conditions would have lasted about 40,000 cycles. Thus, the initiation phase for the clad material was also about 3 to 10 percent of the total fatigue life. In the analysis, a 77 μm quarter-circular corner crack was assumed for the initial crack size. From the test data, this particular crack size seems reasonable. The predicted results (dashed-dot curve) agreed well in the early growth period but tended to show slower rates for longer crack lengths for some of the tests. However, results from other tests, which were stopped at about 22,000 cycles, may have
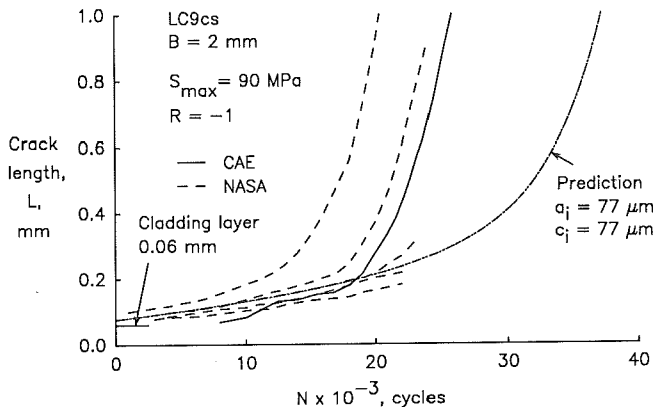
shown better agreement with the prediction if they had been allowed to continue growing. The plastic-replica method did not have an influence on fatigue life for the clad alloy presumably because corner cracks allowed moisture to reach the crack front from the specimen sheet surface.

Small-Crack Growth Rate Data

The crack-growth rate (da/dN) data generated with the SENT specimens are presented as a function of the stress-intensity factor range (ΔK). The small-crack growth rate data is compared to large-crack data (dc/dN) generated from CCT specimens under the same loading conditions. Predictions using the ΔK_{eff}-rate relations and the crack-closure model are compared with the test data.

The calculation of the stress-intensity factor assumes either a semi-elliptical surface crack located at the center of the edge notch, as shown in Figure 2(b), or a quarter-elliptical corner crack located at an edge, as shown in Figure 2(c). For surface cracks located at other places along the bore of the notch, the calculation is adequate if the crack is small compared to thickness. However, if several cracks are close to one another then the calculation is in error.

To calculate the stress-intensity factor at the point where the crack intersects the notch surface ($\varphi = \pi/2$), the crack depth (a) and the crack length (c) must be known. For a surface crack, "2a" (or L) was measured as the projection of the crack on a horizontal plane, as shown in Figure 3. The crack aspect ratio (a/c) and crack length (c) were then calculated from

$$a/c = 1 + 0.1 \ (a/t) \quad \text{for } a/t \geq 0.02 \quad (7a)$$
and
$$a/c = 40 \ (a/t) + 0.2 \quad \text{for } a/t < 0.02 \quad (7b)$$

Similarly, for a corner crack, "a" (or L) is again the projection of the crack on a horizontal plane, as shown in Figure 3(b), and the crack aspect ratio was calculated from

$$a/c = 1.1 + 0.1 \ (a/t) \quad (8)$$

for crack depth (a) greater than the cladding-layer thickness (ℓ). Equations (7a) and (8) were determined by visual straight-line fits to experimental data. Equation (7b) was selected to approximately match predictions from analyses of cracks initiating at a typical material defect size and shape. The measured crack shapes were compared to those predicted from the stress-intensity factor equations and crack-growth rate properties in Figures 16 and 17.

Figure 19. Comparison of experimental and predicted small corner-crack growth in LC9cs alloy SENT specimens.

The stress-intensity factor range equation for a surface or corner crack located at the notch subjected to uniform remote stress is

$$\Delta K = \Delta S \sqrt{\pi a / Q} \; F_{jn} \qquad (9)$$

where F_{jn} is the boundary-correction factor, as previously defined. For corner cracks that occur in the LC9cs clad alloy, a correction for the cladding was developed to modify the stress-intensity factor range calculation, as previously discussed. The stress range (ΔS) is full range (S_{max} - S_{min}) for constant-amplitude and spectrum loading. For spectrum loading, the highest peak stress is S_{max} and the lowest trough is S_{min}.

The calculation of crack-growth rate for constant-amplitude and spectrum loading for small cracks was a simple point-to-point calculation:

$$da/dN = \Delta a / \Delta N = (a_{i+1} - a_i)/(N_{i+1} - N_i) \qquad (10)$$

where a_i is the crack depth at N_i cycles. The cyclic interval, ΔN, is the interval between replicas. The corresponding stress-intensity factor range (ΔK) is calculated at an average crack depth, a, as

$$a = (a_i + a_{i+1})/2 \qquad (11)$$

with the crack length, c, calculated from equations (7) or (8).

<u>Aluminum Alloy 7075-T6</u>. Small-crack data generated under stress ratios of -1 and 0.5, and under Mini-TWIST are shown in Figures 20 to 22, respectively. The range of stress levels used for each series of tests and predictions are indicated. Results at R = -1 are shown in Figure 20. The data from both laboratories agreed well and are plotted as a combined set. These results show the "classical" small-crack effect, in that the small cracks were growing below the large-crack threshold (dash-dot line at ΔK of about 4 MPa-$\sqrt{m}$). However, recall that the use of the replica method influenced the fatigue life and possibly the fatigue-crack-growth rates. If the replica method had not been used, the crack-growth rates for small cracks would have been expected to be even higher than those shown. At higher ΔK values (larger cracks), the small- and large-crack (dashed-dot line) data tended to merge. The solid curves show predicted results using an initial defect size (a_i, c_i, b) of 3 by 9 by 0.5 μm for various maximum stress levels. All predictions start on the ΔK_{eff} curve because cracks at small voids are assumed to be fully open on the first cycle and ΔK is equal to ΔK_{eff}. The predictions
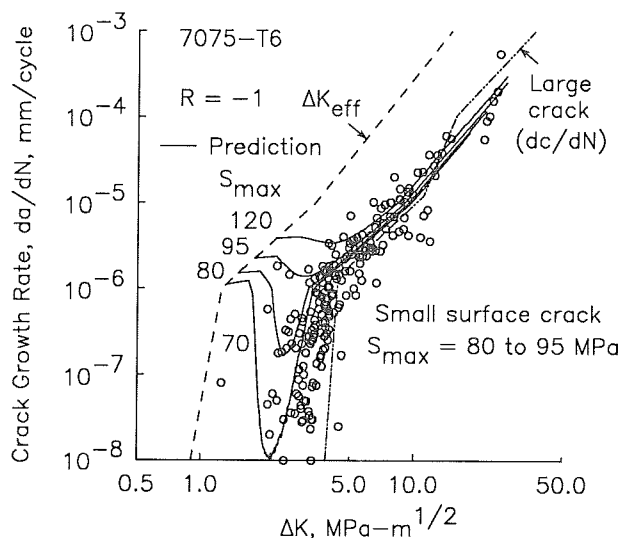

Figure 20. Comparison of experimental and predicted surface-crack-growth rates against ΔK in 7075-T6 alloy SENT specimens at R = -1.

from the model (80 to 95 MPa) did not agree very well with the test data in the near threshold regime. However, the predictions did agree with the test data in the mid- to high-rate range. At 70 MPa, the predictions show that the crack nearly arrested (minimum rate) at a ΔK-value of about 2 MPa-$\sqrt{m}$. At this point the ΔK_{eff} was only slightly greater than 0.9 MPa-$\sqrt{m}$, the effective threshold for small cracks.

Whereas the stress ratio tests with R = 0 and -1 had elastic notch-root stresses, the R = 0.5 test conditions caused the notch root to yield. Under these conditions, small cracks were observed to grow at rates considerably slower than those measured for large cracks at ΔK values greater than the large-crack threshold, as shown in Figure 21. Of course, the influence of the plastic-replica method may be partly responsible for this behavior but the same behavior has been observed for 2024-T3 aluminum alloy, where the replica method did not appear to have a significant effect.[14] The reason for the slower rates for small cracks at R = 0.5 is still under investigation.

A plot of ΔK against rate for small surface cracks under the Mini-TWIST spectrum loading is shown in Figure 22. Note that ΔK was calculated using the highest and lowest stresses in the spectrum sequence. Also, the crack-growth rates are the average rates over about 30,000 cycles. The small-crack data agreed well with the large-crack data. However, this agreement may have been fortuitous because the replica method had a large influence on the fatigue life under Mini-TWIST
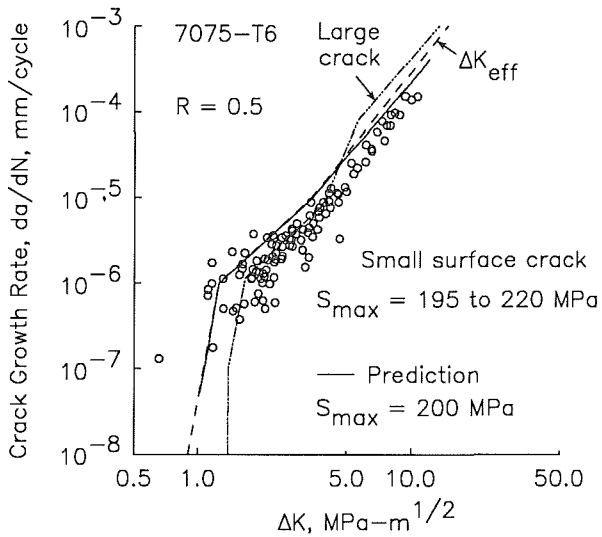
Figure 21. Comparison of experimental and predicted surface-crack-growth rates against ΔK in 7075-T6 alloy SENT specimens at R = 0.5.
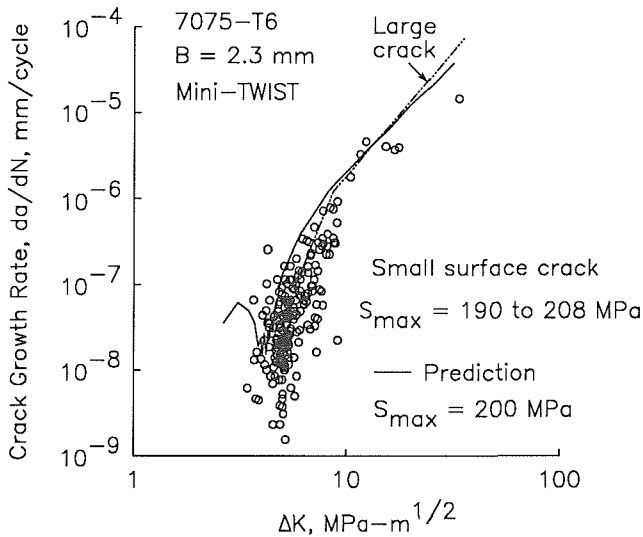

Figure 22. Comparison of experimental and predicted surface-crack-growth rates against ΔK in 7075-T6 alloy SENT specimens under Mini-TWIST loading.

loading (see Ref. 17). Thus, the measured rates may be too low for a given value of ΔK. The predicted crack growth rates were determined in the following way. Crack depth (2a) and cycle results were taken from the analysis at nearly equal cyclic intervals between the initial crack depth and breakthrough (a = t). From these values of crack depth and cycles, the average rate and maximum range stress-intensity factor were calculated. The predicted results (solid curve) showed trends similar to the test data but the predicted rates were, generally, greater than the test data. Again, the plastic-replica method may be responsible for some of the observed differences.

Aluminum Alloy LC9cs. Small-crack tests on the clad alloy primarily produced corner cracks in the core material that initiated from slip-bands in the cladding. Because the cladding yield stress was only about 10 percent of the bare material, the stress distribution at the corner of the notch is complex because the cladding yields and the core material carries most of the load. To calculate the influence of the cladding behavior on stress-intensity factors, a three-dimensional finite-element analysis would be required. In lieu of conducting such an analysis, an engineering estimate was used to develop a simple clad correction to the stress-intensity factors for a corner crack (see the Analytical Program section). The small-crack data generated in the test program was used to evaluate the clad correction.

Some of the small-crack data generated from the LC9cs alloy SENT specimens under stress ratios of -1 and 0 are shown in Figures 23 and 24, respectively. These data were analyzed using the clad correction. The most noticeable difference between 7075-T6 and LC9cs alloys is the growth rates at ΔK values below the large-crack threshold. In the LC9cs alloy, the crack-growth rates were much higher than those measured for the 7075-T6 alloy. Again, some of this difference may have been caused by the influence of the replica method on the 7075-T6 small-crack data. Another source of difference may be the crack sizes and stress levels. The data for the 7075-T6 alloy was generated at much smaller crack sizes than for the LC9cs alloy. The crack sizes in the 7075-T6 ranged from 5 to 100 μm whereas those in the clad material ranged from 80 to 300 μm. Because the model
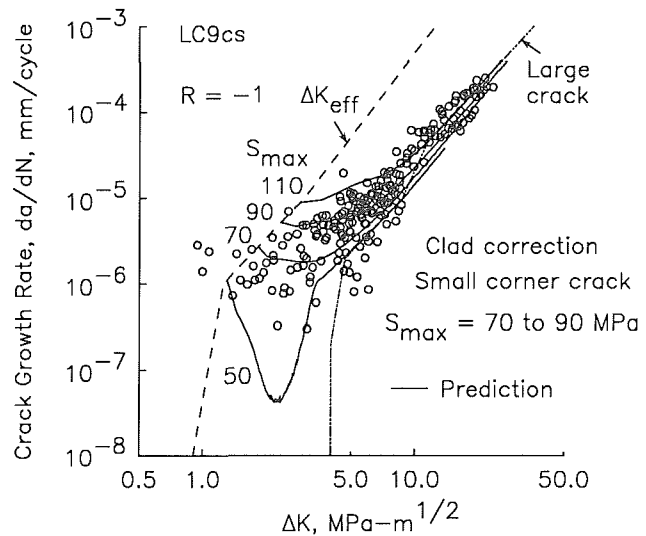

Figure 23. Comparison of experimental and predicted crack-growth rates against ΔK with clad correction in LC9cs alloy SENT specimens at R = -1.

815

predicts a stress level effect, tests conducted on the 7075-T6 alloy at higher stress levels may have shown growth rate data like that shown for the LC9cs alloy.

A comparison of experimental and predicted rates are also shown in Figure 23 for negative stress ratio conditions. The predicted results (solid curves) used an initial crack size of 77 μm and the ΔK_{eff}-rate relations, previously discussed. The predictions from the model agreed well with the test data in the early stages of crack growth. But the predicted rates seem to be slightly low in the mid- to high-rate range. For 50 MPa, the predictions show a large drop in the crack-growth rates, similar to that shown for the 7075-T6 alloy. This behavior is caused by the transient in the crack-closure behavior from the initial crack size to the stabilized value for large cracks, as shown in Figure 7. Crack arrest would have been predicted if an applied stress level of 40 MPa had been used. The fatigue limit for R = -1 was also about 40 MPa (see section on Prediction of Fatigue Life).

Figure 24 shows the results for small surface and corner cracks under R = 0 constant-amplitude loading conditions. The solid and open symbols show data for surface and corner cracks, respectively. In the mid-rate region, all surface-, corner- and through-crack (large-crack) data agreed quite well. The predicted results agreed well with the surface- and corner-crack data. These results strongly support the simple clad correction made to the corner-crack stress-intensity factors.[17]
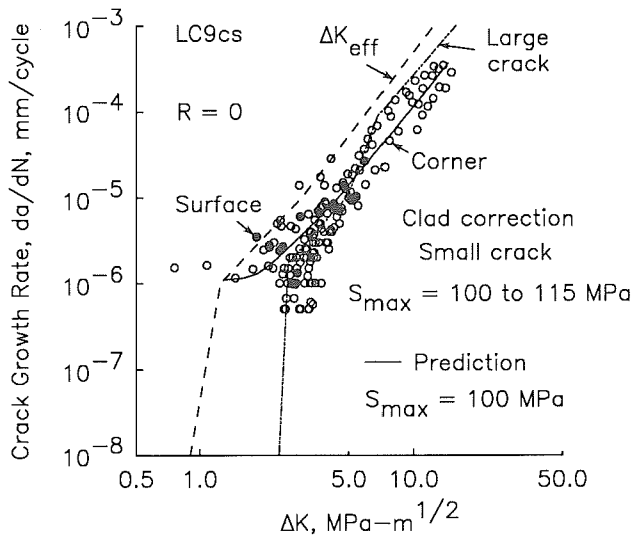

Figure 24. Comparison of experimental and predicted crack-growth rates against ΔK with clad correction in LC9cs alloy SENT specimens at R = 0.

Small-crack data on corner cracks in the LC9cs alloy under the Mini-TWIST spectrum loading are shown in Figure 25. Again, ΔK has been calculated using the highest and lowest stresses in the spectrum and the clad correction. The predicted small-crack growth rates are shown as the solid curve. These predictions agreed well with the test data for both small and large cracks.
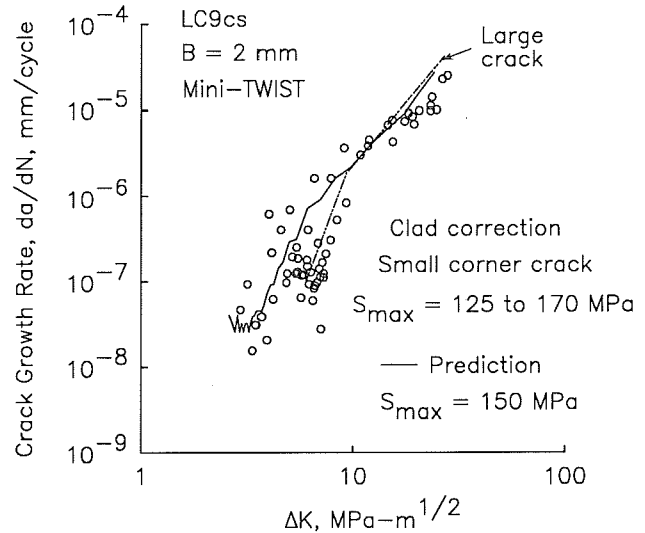

Figure 25. Comparison of experimental and predicted crack-growth rates against ΔK with clad correction in LC9cs alloy SENT specimens under Mini-TWIST loading.

VIII. Prediction of Fatigue Life

In the small-crack tests, crack growth was monitored from 80 to 97 percent of the total fatigue life. Thus, all of the elements are in place to assess a total fatigue-life prediction method based solely on crack propagation from microstructural features, such as the inclusion-particle clusters (or voids) and the cladding layer. The fatigue tests that were conducted in the early part of the cooperative program will now be used in this assessment. In this approach, a crack is assumed to initiate and grow at the notch root on the first cycle. The crack-closure model and the baseline ΔK_{eff}-rate curves are used to predict crack growth from the initial crack size to failure. These predictions will be compared with fatigue lives obtained from SENT specimens. Because these tests were standard fatigue tests, the effects of the plastic-replica method on fatigue life for the 7075-T6 alloy will not be an issue.

Constant-Amplitude Loading

Fatigue life (S-N) data under constant-amplitude loading are shown in Figures 26 and 27 for the 7075-T6 and LC9cs alloys, respectively. A plain symbol indicates a failure and a symbol with an arrow indicates that a test was terminated before failure. In the analysis, an initial crack size of $a_i = 3$ μm, $c_i = 9$ μm and b = 0.5 μm was assumed for the 7075-T6 alloy. This crack size is very close to the average defect size that was measured at the crack initiation sites. For the clad alloy, an initial corner-crack size of $a_i = 77$ μm, $c_i = 77$ μm and b = 0.5 μm was used. This crack size is somewhat larger than the cladding layer thickness, but is consistent with the smallest crack sizes observed early in life (see Fig. 19). In these tests, the clad alloy exhibited more scatter than the 7075-T6 alloy, especially at the high stress ratio condition. The effective stress-intensity factor threshold $(\Delta K_{eff})_{th}$ was 0.9 MPa-$\sqrt{m}$ for both alloys. Using the crack-closure model and life-prediction code, predictions were made for all loading conditions. The solid curves show the predicted number of cycles to failure. The predicted lives were in reasonable agreement with the test lives. In addition to predicting fatigue life, the analysis methodology was also able to predict the fatigue limit as a function of stress ratio.
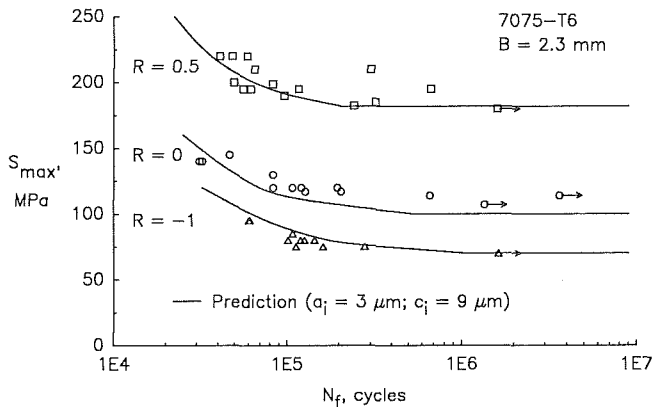

Figure 26. Comparison of experimental and predicted fatigue lives for 7075-T6 alloy SENT specimens for various stress ratios.

Mini-TWIST Loading

Experimental and predicted results for the Mini-TWIST spectrum loading on the 7075-T6 and LC9cs clad alloy SENT specimens are shown in Figure 28. The solid and dashed curves show predictions for each alloy using the same initial defects as used for constant-amplitude loading. The predicted lives were in reasonable agreement with the test results (symbols) but the predicted lives tended to fall on the lower bound of the test data.
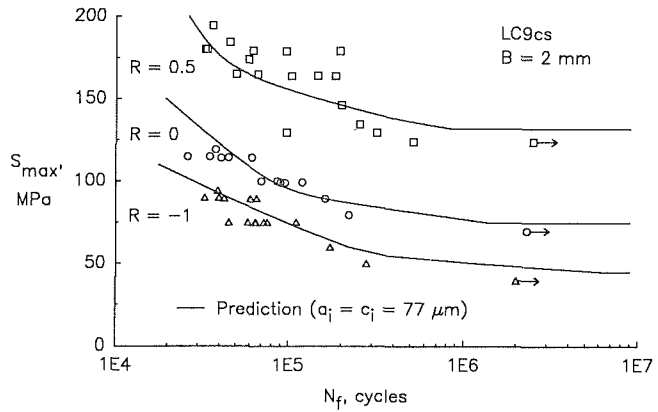

Figure 27. Comparison of experimental and predicted fatigue lives for LC9cs alloy SENT specimens for various stress ratios.
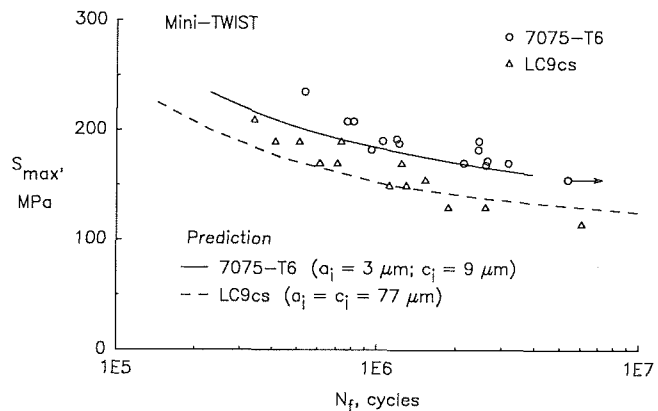

Figure 28. Comparison of experimental and predicted fatigue lives for 7075-T6 and LC9cs alloys under Mini-TWIST loading.

IX. Conclusions

The National Aeronautics and Space Administration (NASA) and the Chinese Aeronautics and Astronautics Establishment (CAE) participated in a Fatigue and Fracture Mechanics Cooperative Program. The program objectives were to study the "small-crack" effect in two high-strength aluminum alloys, to compare experimental and analytical results from each laboratory, and to evaluate an existing model to predict the growth of such cracks. Experimental and analytical studies were conducted on various aspect of the fatigue crack growth of small and large cracks. Small-crack tests and analyses conducted on single-edge-notched tension (SENT) fatigue specimens made of 7075-T6 bare and LC9cs clad aluminum alloy sheet materials support the following:

Analytical Results

1. Stress-intensity factor solutions for surface and corner cracks at a notch determined by the three-dimensional finite-element method and the weight-function method generally agreed within ± 3 percent over a wide range in crack-configuration parameters. The finite-element method required a large mainframe computer whereas the weight-function method used a personal computer.

2. Stress-intensity factor solutions for a through crack at a notch in a plate subjected to remote uniform stress or displacement were determined by a two-dimensional boundary-force method. Remote uniform displacement boundary conditions were confirmed using an experimental technique.

3. Stress-intensity factor equations were developed for surface, corner and through cracks at a notch for a wide range in crack-configuration parameters.

4. A simple clad correction to estimate the influence of the low-yield cladding material on stress-intensity factors for a corner crack at the notch was developed from a two-dimensional weight-function method.

Experimental Results

1. Fatigue lives and small-crack growth rates measured on single-edge-notch-tension specimens under constant-amplitude and Mini-TWIST spectrum loading from both laboratories agreed well for all loading conditions.

2. Large-crack growth rates measured under three constant-amplitude stress ratios (R = -1, 0 and 0.5) from both laboratories agreed well over a wide range in rates. Some slight discrepancies were observed in the threshold regime.

3. For both materials, small cracks grew below the large-crack threshold especially for the lower stress ratio tests. Small-crack effects were shown to be more pronounced for the negative stress ratio tests.

4. For the 7075-T6 alloy, surface cracks initiated at inclusion-particle clusters or voids at or near the notch surface. Over 70 percent of the cracks initiated in the middle half of the sheet specimen thickness.

5. For the LC9cs clad alloy, corner cracks initiated from slip-band formation in the cladding layers. Over 90 percent of the cracks initiated at the edges of the notch and sheet surfaces.

6. For both materials, results from both laboratories showed that most of the fatigue life (80 to 97 percent) was crack propagation from a microstructural material defect (inclusion particles or voids) or the cladding layer.

7. Measured crack-growth rates for large surface and corner cracks at the notch indicated that the crack-growth properties in the thickness and width directions were different for both alloys.

Crack-Closure Model

1. For both materials, the crack-closure concept correlated large-crack-growth rate against the effective stress-intensity factor range over six to eight orders-of-magnitude in rate for the three constant-amplitude stress ratio (R = -1, 0 and 0.5) conditions.

2. For constant-amplitude and Mini-TWIST spectrum loading, the crack-closure model predicted crack-growth rates for small cracks like those observed experimentally, especially for the LC9cs clad alloy. Some of the discrepancies observed for the 7075-T6 alloy were attributed to the effects of the plastic-replica method (acetone) influence on small-crack growth rates.

3. The crack-closure model predicted the crack-length-against-cycles curve for a large crack in a plate subjected to the Mini-TWIST spectrum loading generally within about ± 20 percent for both alloys.

4. Using a microstructural feature (inclusion-particle size) or nearly the cladding-layer thickness as an initial defect, a total fatigue life prediction method was demonstrated using the crack-closure model.

   The cooperative program demonstrated that international cooperation between research organizations can be very fruitful. The cooperative program has advanced the state-of-the-art in fatigue and fracture mechanics and has provided the aerospace industries with useful experimental data and with efficient analysis methods for improving life prediction. These results should ultimately improve the reliability and safety of aircraft structures.

X. References

1. Pearson, S.: Engng. Fract. Mech., Vol. 7, No. 2, 1975, pp. 235-247.

2. Kitagawa, H.; and Takahashi,S.: in Proceedings 2nd Int. Conf. on Mechanical Behavior of Materials, Boston, MA, 1976, pp. 627-631.

3. El Haddad, M. H.; Dowling, N. E.; Topper, T. H.; and Smith, K. N.: Int. J. of Fracture, Vol. 16, No. 1, 1980, pp. 15-30.

4. Hudak, S. J., Jr.: J. Engng. Materials and Technology, Vol. 103, 1981, pp. 26-35.

5. Nisitani, H.; and Takao,K. I.: Engng. Fract. Mech., Vol. 15, No. 3, 1981, pp. 445-456.

6. Schijve, J.: in Fatigue Thresholds, Vol. II, 1982, pp. 881-908. (Also: Delft University of Technology Report LR-327, 1981.)

7. Lankford, J.: Fatigue of Engng. Materials and Structures, Vol. 5, No. 3, 1982, pp. 233-248.

8. Wood, H. A.; and Rudd, J. L.: Evaluation of Small Cracks in Airframe Structures, AGARD Report No. 696, 1983, pp. 1.1-1.12.

9. Newman, J. C., Jr.: A Nonlinear Fracture Mechanics Approach to the Growth of Small Cracks, Behaviour of Short Cracks in Airframe Components, AGARD CP-328, 1983, pp. 6.1-6.26.

10. Leis, B. N.; Kanninen, M. F.; Hopper, A. T.; Ahmad, J.; and Broek, D.: A Critical Review of the Short Crack Problem in Fatigue, AFWAL-TR-83-4019, 1983.

11. The Behaviour of Short Fatigue Cracks, Miller, K. J. and de los Rios, E. R., eds., European Group on Fracture, Publication No. 1, 1986.

12. Small Fatigue Cracks, Ritchie, R. O. and Lankford, J., eds., The Metallurgical Society, 1986.

13. Phillips, E. P.; and Newman, J. C., Jr.: Experimental Mechanics, June 1989, pp. 221-225.

14. Newman, J. C., Jr.; and Edwards, P. R.: Short-Crack Growth Behaviour in an Aluminum Alloy - An AGARD Cooperative Test Programme, AGARD R-732, 1988.

15. Short-Crack Growth Behaviour in Various Aircraft Materials, Edwards, P. R. and Newman, J. C., Jr., eds., AGARD R-767, 1990.

16. Small Crack Test Methods, ASTM STP 1149, J. Allison and J. Larsen, eds., Philadelphia, 1992, pp. 6-33.

17. Newman, J. C., Jr.; Wu, X. R.; Venneri, S. L.; and Li, C. G.: A Fatigue and Fracture Mechanics Cooperative Program on Small-Crack Effects in High-Strength Aluminum Alloys, NASA RP in preparation, 1992.

18. Tan, P. W.; I. S. Raju; and J. C. Newman, Jr.: in Fracture Mechanics: Eighteenth Symposium, ASTM STP 945, D. T. Read and R. P. Reed, eds., Philadelphia, 1988, pp. 259-277.

19. Newman, J. C. Jr.: in Methods and Models for Predicting Fatigue Crack Growth Under Random Loading, ASTM STP 748, J. B. Chang and C. M. Hudson, eds., Philadelphia, 1981, pp. 53-84.

20. Elber, W.: in Damage Tolerance in Aircraft Structures, ASTM STP 486, Philadelphia, 1971, pp. 230-242.

21. Lowak, H.; deJonge, J. B.; Franz, J.; and Shutz, D.: MINITWIST - A Shortened Version of TWIST, Laboratorium fur Betrieksfestigkeit (LBF), Report No. TB-146 (1979) or Nationaal Lucht-En Ruimtevaartlaboratorium (NLR), NLR MP-79018U (1979).

22. Brown, C. W.; and Smith, G. C.: in Advances in Crack Length Measurement, C. J. Beevers, ed., Engng. Materials Advisory Services Ltd., 1982, pp. 41-51.

23. Raju, I. S.; and Newman, J. C., Jr.: Engng. Fract. Mech., Vol. 11, No. 4, 1979, pp. 817-829.

24. Raju, I. S.; and Newman, J. C., Jr.: in Fracture Mechanics, ASTM STP 677, C. W. Smith, ed., Philadelphia, 1979, pp. 411-430.

25. Newman, J. C., Jr.; and Raju, I. S.: in Fracture Mechanics Fourteenth Symposium, ASTM STP 791, J. C. Lewis and G. Sines, Eds., 1983, pp. I238-I265.

26. Nikishkov, G. P.; and Atluri, S. N.: Engng. Fract. Mech., Vol. 26, 1987, pp. 851-867.

27. Shivakumar, K. N.; Tan, P. W.; and Newman, J. C., Jr.: Int. J. of Fracture, Vol. 36, 1988, pp. R43-R50.

28. Tan, P. W.; Raju, I. S.; Shivakumar, K. N.; and Newman, J. C., Jr.: in Surface-Crack Growth: Models, Experiments and Structures, ASTM STP 1060, W. G. Reuter, J. H. Underwood, and J. C. Newman, Jr., eds., Philadelphia, 1990, pp. 34-48.

29. Shivakumar, K. N.; and J. C. Newman, Jr.: Engng. Fract. Mech., Vol. 38, No. 6, 1991, pp. 467-473.

30. Swain, M. H.; and Newman, J. C., Jr.: in Fatigue Crack Topography, AGARD CP No. 376, 1984, pp.12.1-12.17.

31. Zhao, W.; Wu, X. R.; and Yan, M. G.: Engng. Fract. Mech., Vol. 34, 1989, pp. 593-607.

32. Zhao, W.: Weight Function Theory and Application for Analysis of Three Dimensional Crack Problems, Ph.D. Thesis, Institute of Aeronautical Materials, 1988.

33. Fujimoto, W. T.: in Proceedings AIAA/ASME/SAE 17th Structures, Structural Dynamics, and Material Conference, King of Prussia, PA, May 5-7, 1976.

34. Saff, C. R.; and Sanger, K. B.: in Fracture Mechanics: Fifteenth Symposium, ASTM STP 833, R. J. Sanford, ed., Philadelphia, 1984, pp. 24-43.

35. Wu, X. R.; and Carlsson, J.: J. of Mech. and Phys. of Solids, Vol. 31, 1983, pp. 485-497.

36. Wu, X. R.: Engng. Fract. Mech., Vol. 20, 1984, pp. 35-49.

37. Wu, X. R.: Weight Functions and Stress-Intensity Factors for Radial Crack(s) Emanating from a Circular Hole in an Infinite Sheet, The Royal Institute of Technology, Report 63, Stockholm, Sweden, 1985.

38. Wu, X. R. and Carlsson, A. J.: Weight Functions and Stress Intensity Factor Solutions, Pergamon Press, Inc., 1991.

39. Zhao, W.; Wu, X. R.; and Yan, M. G.: Engng. Fract. Mech., Vol. 34, No. 3, 1989, pp. 593-607.

40. Zhao, W.; and Wu, X. R.: Theoretical and Applied Fract. Mech., Vol. 13, 1990, pp. 225-238.

41. Zhao, W.; and Wu, X. R.: Fatigue and Fract. of Engng. Materials and Structures, Vol. 13, 1990, pp.347-360.

42. Folias, E. S.: in _Fracture Mechanics: Nineteenth Symposium_, ASTM STP 969, T. A. Cruse, ed., Philadelphia, 1988, pp. 56-72.

43. Erdogan, F.: in Proceedings 4th U. S. Nat. Cong. of Applied Mech., 1962, pp. 547-553.

44. L. A. James; and W. E. Anderson: Engng. Fract. Mech. J., Vol. 1, 1969, pp. 565-568.

45. Newman, J. C., Jr.: FASTRAN II - A Fatigue Crack Growth Structural Analysis Program, NASA TM 104159, February 1992.

46. Tada, H.; Paris, P. C.; and Irwin, G. R.: _The Stress Analysis of Cracks Handbook_, Del Research Corporation, 1985.

47. Newman, J. C., Jr.; Swain, M. H.; and Phillips, E. P.: in _Small Fatigue Cracks_, R. O. Ritchie and J. Lankford, eds., The Metallurgical Society, 1986, pp. 427-452.

48. Newman, J. C., Jr.; Poe, C. C., Jr.; and Dawicke, D. S.: in Proceedings of 4th Int. Conf. on Fatigue and Fatigue Thresholds, Honolulu, Hawaii, July 1990, pp. 2407-2416.

49. Newman, J. C., Jr.: Int. J. of Fract., Vol. 24, 1984, R131-R135.

50. Newman, J. C., Jr.; and Raju, I. S.: in _Advances in Fracture Research_, Pergamon Press, 1985, pp. 1597-1608.

51. Yoder, G. R.; Cooley, L. A.; and Crooker, T. W.: On Microstructural Control of Near-Threshold Fatigue Crack Growth in 7000-Series Aluminum Alloys, NRL MR 4787, Naval Research Laboratory, Washington, D. C., April 1982.

52. Wanhill, R. J. H.: Engng. Fract. Mech., Vol. 30, 1988, pp. 233-260.

53. Irwin, G. R.: Plastic Zone Near a Crack and Fracture Toughness, Proceedings of the 7th Sagamore Conference, 1960, p. IV-63.

54. Vogelesang, L. B.: The Effect of Environment on the Transtition from Tensile Mode to Shear Mode during Fatigue Crack Growth in Aluminum Alloys, Delft University of Technology, Report LR-286, October 1979.

55. Schijve, J.: in _Fatigue Crack Propagation_, ASTM STP 415, 1967, pp. 415-457.

56. Minakawa, K.; and McEvily, A. J.: in _Fatigue Thresholds_, Vol I, 1982, pp. 373-390.

57. Bowles, C. Q.; and Schijve, J.: Int. J. of Fract., Vol. 9, No. 2, 1973, pp. 171-179.

58. Schijve, J.; Jacobs, F. A.; and Tromp, P. J.: The Significance of Cladding for Fatigue of Alumunum Alloys in Aircraft Structures, National Aerospace Laboratory, NLR TR 76065U, 1976.